

We are IntechOpen, the world's leading publisher of Open Access books Built by scientists, for scientists

4,800

Open access books available

122,000

International authors and editors

135M

Downloads

Our authors are among the

154

Countries delivered to

TOP 1%

most cited scientists

12.2%

Contributors from top 500 universities



WEB OF SCIENCE™

Selection of our books indexed in the Book Citation Index
in Web of Science™ Core Collection (BKCI)

Interested in publishing with us?
Contact book.department@intechopen.com

Numbers displayed above are based on latest data collected.

For more information visit www.intechopen.com



Improved DTC Algorithms for Reducing Torque and Flux Ripples of PMSM Based on Fuzzy Logic and PWM Techniques

Khalid Chikh, Mohamed Khafallah and Abdallah Saâd

Additional information is available at the end of the chapter

<http://dx.doi.org/10.5772/48503>

1. Introduction

Permanent Magnet Synchronous Motors (PMSM's) are widely used in high-performance drives such as industrial robots, automotive hybrid drive trains and machine tools thanks to their advantages as: high efficiency, high power density, high torque/inertia ratio, and free maintenance. In the recent years, the magnetic and thermal capabilities of the Permanent Magnet (PM) have been considerably increased by employing the high-coercive permanent magnet material.

Direct Torque Control (DTC) method has been first proposed and applied for induction machines in the mid-1980s, by Takahachi and Noguchi, for low and medium power applications. This concept can also be applied to synchronous drives. Indeed, PMSM DTC has appeared in the late 1990s. However, for some applications, the DTC has become unusable although it significantly improves the dynamic performance (fast torque and flux responses) of the drive and is less dependent on the motor parameters variations compared to the classical vector control due to torque and flux ripples. Indeed, hysteresis controllers used in the conventional structure of the DTC generates a variable switching frequency, causing electromagnetic torque oscillations. Also this frequency varies with speed, load torque and hysteresis bands selected. In addition, a high sampling frequency is needed for digital implementation of hysteresis comparators and a current and torque distortion is caused by sectors changes.

In the last decade, several contributions have been proposed to overcome these problems by using the three level or the multilevel inverter: more voltage space vectors are available to control the flux and torque. However, more power switches are needed to achieve a lower

ripple and almost fixed switching frequency, which increases the system cost and complexity. In order to improve the DTC performance and overcome the above cited problems, another solution combines basic DTC and fuzzy logic control advantages in one control strategy, named Fuzzy Direct Torque Control (FDTC). In this technique, the hysteresis comparator and the switching table used in basic DTC are replaced by a fuzzy logic switcher, which decides directly on the switches states of the Voltage Source Inverter (VSI). In addition, it's known that fuzzy control works as well for complex non-linear multi-dimensional system, system with parameter variation problem and/or cases where the sensor signals are not precise. The fuzzy control is basically nonlinear and adaptive in nature, giving robust performance under parameter variation and load disturbance effect. For all these reasons, a Fuzzy Logic Controller can be used instead of the speed PI controller in FDTC in order to achieve a complete fuzzy control for the PMSM. Also, much interest has been focused on the use of modified DTC structures to improve basic DTC performances by replacing the hysteresis controllers and the switching table by a PI regulator, predictive controller and Space Vector Modulation (SVM). Indeed, under DTC-SVM strategy, both torque and flux linkage ripples are greatly reduced when compared with those of the basic DTC, because the application of SVM guarantees lower harmonics current by eliminating the distortion caused by sector changes in case of DTC switching table and by fixing the switching frequency.

Moreover, the design of the speed controller used in basic DTC or in modified DTC strategies, greatly affects the performance of the drive. The PI controllers have a simple structure and can offer satisfactory performances over a wide range of operations. However, due to the uncertainties, the variations in the plant parameters and the nonlinear operating conditions, the fixed gains of the PI controller may become unable to provide the required control performance. In order, to realize a good dynamic behaviour of the PMSM, a perfect speed tracking with no overshoot and a good rejection of impact loads disturbance, the speed PI controller can be replaced by a PI-Fuzzy speed controller.

This chapter is organized as follows: PMSM modelling and simulation results of the basic DTC by using Matlab/Simulink environment with a simple speed PI corrector, will be presented and discussed in Section 2 and 3, respectively. Whereas in Section 4 a complete Fuzzy Direct Torque Control (FDTC), which uses a fuzzy switching table and a PI-Fuzzy speed controller, for PMSM is proposed to reduce the torque and flux ripples. In addition, the simulation results show the effectiveness of this strategy when compared with the basic DTC and a classical speed PI controller. Section 5 and 6 are devoted to presenting a fixed switching-frequency DTC with two approaches: Sinusoidal Pulse With Modulation (SPWM) and Space Vector Modulation (SVM). The objective, of these two strategies, is reducing the flux and torque ripples and fixing the switching-frequency. Of course, the simulation results of these two approaches will be discussed and compared with those of basic DTC and FDTC, in section 7. Section 8 is devoted to study DTC performances under PMSM parameters variation, also a solutions have been proposed to overcome this issue. Eventually, conclusion and simulation results interpretations are included in Section 9.

2. Modelling of the VSI and the PMSM

2.1. Voltage Source Inverter (VSI) for adjustable speed or torque drive

In large number of industries the PMSM's are required to be operated at different speeds or torques. In order to obtain variable speed or torque, these motors are fed from inverters with variable voltage and variable frequency supply. Figure 1 shows the VSI structure used to produce well the voltage waveforms at the terminal of the motor. The voltage control of this inverter is obtained by using switching table in case of basic DTC or by pulse width modulation (PWM) in case of modified DTC techniques.

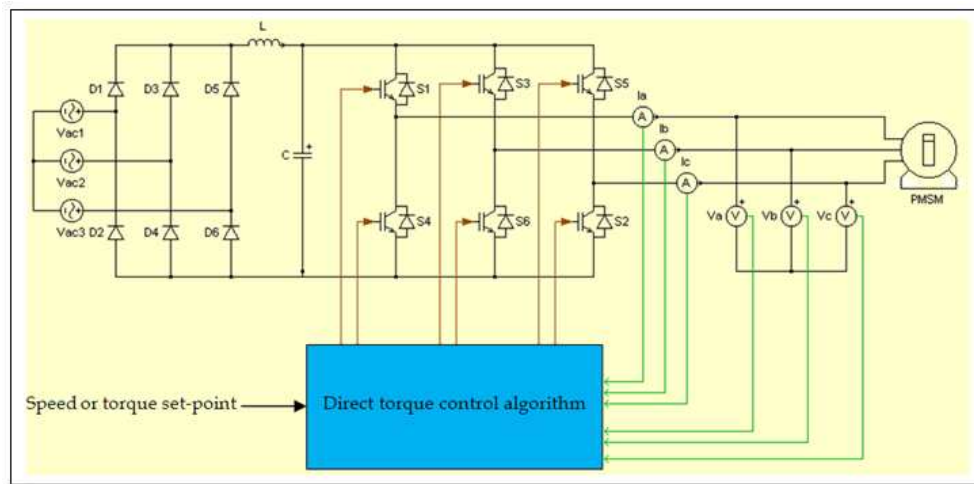


Figure 1. Three phase voltage source bridge inverter structure

The model of the VSI is given by:

$$\begin{bmatrix} V_a \\ V_b \\ V_c \end{bmatrix} = \frac{U_{dc}}{3} \begin{bmatrix} 2 & -1 & -1 \\ -1 & 2 & -1 \\ -1 & -1 & 2 \end{bmatrix} \begin{bmatrix} C_{S1} \\ C_{S3} \\ C_{S5} \end{bmatrix} \quad (1)$$

Where U_{dc} is the DC bus voltage and C_{s1} , C_{s3} , C_{s5} are the transistor states.

2.2. Modeling of the PMSM

The stator voltages equation for a PMSM in the rotor oriented coordinates d-q can be expressed as:

$$\begin{bmatrix} U_{sd} \\ U_{sq} \end{bmatrix} = \begin{bmatrix} R_s + s \cdot L_d & -P \cdot \omega_m \cdot L_q \\ P \cdot \omega_m \cdot L_d & R_s + s \cdot L_q \end{bmatrix} \begin{bmatrix} I_{sd} \\ I_{sq} \end{bmatrix} + \begin{bmatrix} 0 \\ P \cdot \omega_m \cdot \Phi_{PM} \end{bmatrix} \quad (2)$$

Where I_{sd} and I_{sq} are the d - q axis stator currents, R_s is the stator resistance, Ψ_{PM} is the flux linkage of the rotor magnets linking the stator, L_d and L_q are the d - q axis stator inductances, P is the number of pole pairs and ω_m is the mechanical speed.

And the electromagnetic torque equation in the rotor oriented coordinates d-q can be expressed as (3):

$$\Gamma_{em} = \frac{3}{2}P(\Phi_{sd}I_{sq} - \Phi_{sq}I_{sd}) = \frac{3}{2}P[\Phi_{PM}I_{sq} + (L_d - L_q)I_{sd}I_{sq}] \tag{3}$$

Where Φ_{sd} and Φ_{sq} are d - q components of the stator flux linkage, which are expressed as:

$$\begin{bmatrix} \Phi_{sd} \\ \Phi_{sq} \end{bmatrix} = \begin{bmatrix} L_d & 0 \\ 0 & L_q \end{bmatrix} \begin{bmatrix} I_{sd} \\ I_{sq} \end{bmatrix} + \begin{bmatrix} \Phi_{PM} \\ 0 \end{bmatrix} \tag{4}$$

Finally, when the dry friction torque is neglected; the motion equation is expressed as:

$$J \frac{d\omega_m}{dt} = \Gamma_{em} - \Gamma_r - f_r \omega_m \tag{5}$$

Where J moment of inertia, Γ_r motor load and f_r damping constant.

3. Basic direct torque control for PMSM

DTC is a vector control method used to control the torque and therefore the speed of the motor by controlling the switching sequence of the inverter transistors. Figure 2 shows the DTC for a PMSM block diagram. It can be seen that once one has the estimated and reference instantaneous values of electromagnetic torque and stator flux, we proceed to calculate the error between them; these errors are used as inputs for the hysteresis controllers, which aim to maintain the torque and flux errors within upper and lower limits allowed, so that when evaluating within these limits an output level is obtained to know the status of the variable. The output levels achieved in this stage of the control are input signals to the block that is responsible for finding the right vector to get rid of the speed error. This procedure is made for each sampling instant to drive the PMSM to the desired speed value.

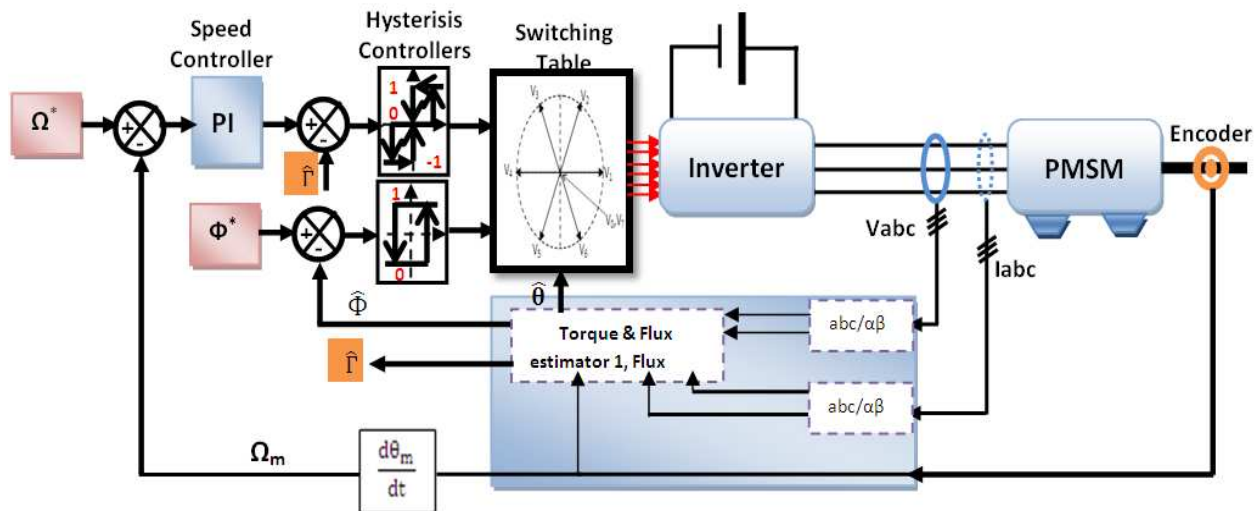


Figure 2. DTC scheme for PMSM with Classical Torque and Flux Estimator (CTFE)

In the DTC, the motor torque control is achieved with two hysteresis controllers, one for stator flux magnitude error and the other for the torque magnitude error. The selection of one switching vector per sampling time depends on the sign of these two controllers without inspections of the magnitude of the errors produced in the transient and dynamic situations per sampling time and level of the applied stator voltage.

3.1. Stator flux control

The stator voltage vector equation, in a stator reference frame, is given by:

$$\overline{V}_s = R_s \cdot \overline{I}_s + \frac{d\overline{\Phi}_s}{dt} \quad (6)$$

Where R_s is the stator resistance and $\overline{V}_s = V_{s\alpha} + jV_{s\beta}$.

So

$$\overline{\Phi}_s = \overline{\Phi}_0 + \int_0^t (\overline{V}_s - R_s \cdot \overline{I}_s) dt \quad (7)$$

For high speeds, the term $R_s \cdot \overline{I}_s$ can be neglected, so the equation 7 is given by:

$$\overline{\Phi}_s \approx \overline{\Phi}_0 + \int_0^t \overline{V}_s dt \quad (8)$$

$\overline{\Phi}_0$ is the initial stator flux at the instant t_0 .

Because during one sampling period T_e the selected stator voltage vector is always constant, the last equation becomes:

$$\overline{\Phi}_s(k+1) \approx \overline{\Phi}_s(k) + \overline{V}_s \cdot T_e \quad (9)$$

$$\Delta\overline{\Phi}_s = \overline{V}_s \cdot T_e = \overline{\Phi}_s(k+1) - \overline{\Phi}_s(k) \quad (10)$$

With: T_e is the sampling period.

$\overline{\Phi}_s(k)$ is the stator flux vector at the actual sampling period.

$\overline{\Phi}_s(k+1)$ is the stator flux vector at the next sampling period.

$\Delta\overline{\Phi}_s$ is the variation of stator flux vector.

From equation 10, it is seen that the variation of the stator flux is directly proportional to the stator voltage; consequently the control is carried out by varying the stator flux vector by selecting a suitable voltage vector with the Voltage Source Inverter (VSI).

Figure 3 shows that the stator flux vector is varied in the same direction as the applied stator voltage vector. Therefore, applied a collinear stator voltage vector as the stator flux vector and in the same direction as it is a sufficiently condition to increase it, and vice versa. Indeed, to control the stator flux vector $\overline{\Phi}_s(k)$ an estimator of its module $\widehat{\Phi}_s$ and its argument $\widehat{\theta}_s$ is needed; the stator flux can be estimated from the measure of stator currents and voltages and their transformation in the $\alpha\beta$ subspace, by integrating of difference between the input voltage and the voltage drop across the stator resistance as given by:

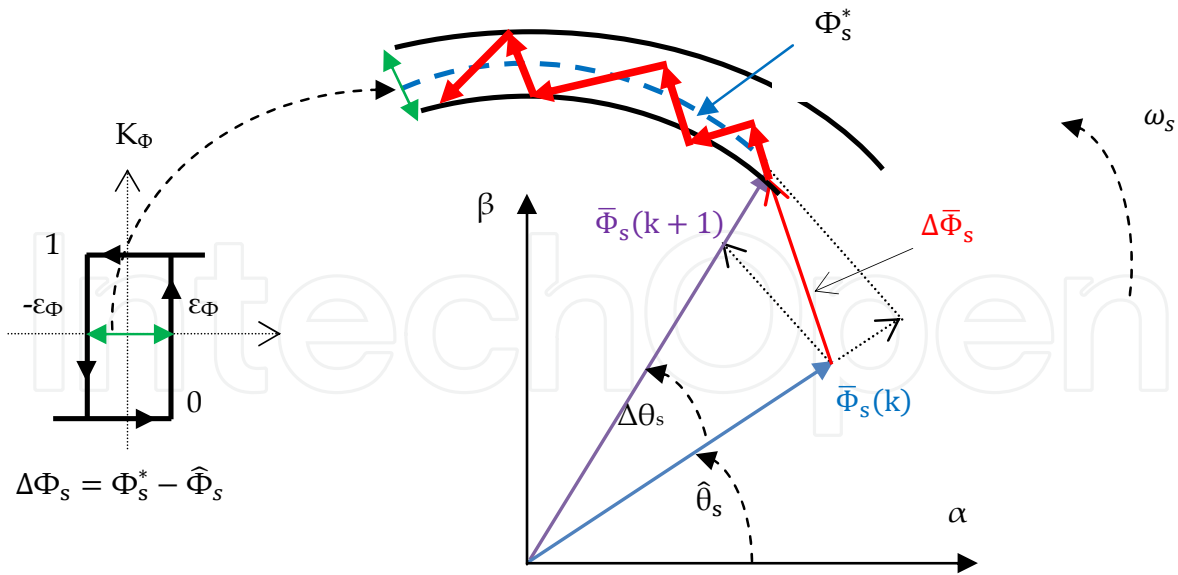


Figure 3. Stator flux vector evolution in the $\alpha\beta$ subspace

$$\Phi_{s\alpha} = \Phi_{PM} + \int_0^t (V_{s\alpha} - R_s \cdot I_{s\alpha}) dt \quad (11)$$

$$\Phi_{s\beta} = \int_0^t (V_{s\beta} - R_s \cdot I_{s\beta}) dt \quad (12)$$

Note that Φ_{PM} is the permanent magnet flux. From equations 11 and 12, the stator flux module and its argument are given by:

$$\hat{\Phi}_s = \sqrt{\Phi_{s\alpha}^2 + \Phi_{s\beta}^2} \quad (13)$$

$$\hat{\theta}_s = \tan^{-1}\left(\frac{\Phi_{s\beta}}{\Phi_{s\alpha}}\right) \quad (14)$$

A two level hysteresis controller, as indicated in figure 3, is used to control the stator flux, which compares the reference stator flux Φ_s^* with the estimated stator flux $\hat{\Phi}_s$. The flux hysteresis comparator output is denoted by Boolean variable K_Φ which indicates directly if the amplitude of flux must be increased $K_\Phi = 1$ or decreased $K_\Phi = 0$: if $K_\Phi = 1$, it means that the actual value of the flux linkage is below the reference value and outside the hysteresis limit; so the stator flux must be increased, while if $K_\Phi = 0$, it means that the actual value of the flux linkages is above the reference value and outside the hysteresis limit; so the stator flux must be decreased.

The two level VSI, as shown in figure 1, is used to select proper voltage vectors from the output of flux and torque hysteresis controller (will be presented in the next part). The inverter has eight permissible switching states ($V_0, V_1 \dots V_7$), out of which six are active ($V_1, V_2 \dots V_6$) and two zero or inactive states (V_0 and V_7). The voltage vector plane is divided into six sectors so that each voltage vector divides each region in two equal parts as shown in Figure 4. In each sector four of the six non-zero voltage vectors along with zero vectors may be used.

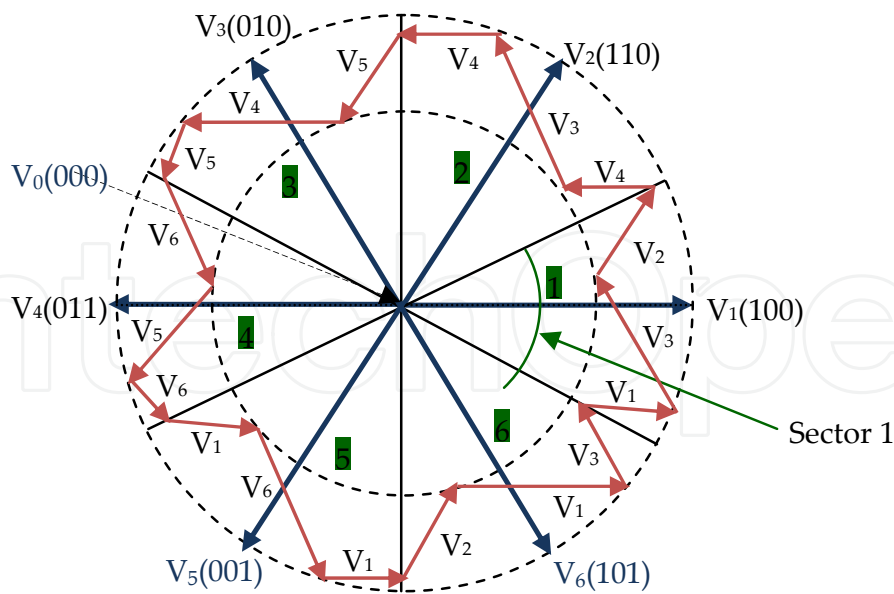


Figure 4. Control of stator flux by selection of the suitable voltage vector $V_{i(i=0,\dots,7)}$

3.2. Torque control

The electromagnetic torque equation is defined as follows:

$$\Gamma = k \cdot (\bar{\Phi}_s \cdot \bar{\Phi}_r) = \|\bar{\Phi}_s\| \cdot \|\bar{\Phi}_r\| \cdot \sin \delta \tag{15}$$

Where δ is the angle between the rotor and the stator flux vectors and the constant k is expressed as (when $L_d = L_q$):

$$k = \frac{3P}{2L_q}$$

The equation 15 indicates that the electromagnetic torque depends to the rotor and stator amplitude, and the angle δ . So, if the stator flux vector is perfectly controlled, by mean of the stator voltage vector \bar{V}_s , in module and in position; consequently, the electromagnetic torque can be controlled by the same stator voltage vector.

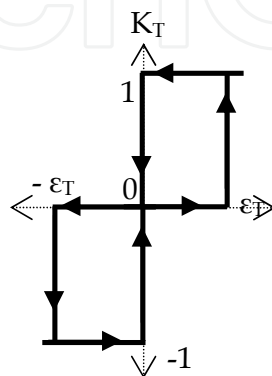


Figure 5. Three level hysteresis controller

Note that the electromagnetic torque can be controlled by mean of a two level comparator as the same as stator flux (see figure 3) or by using a three level comparator as shown in figure 5. In this work, a three level comparator has been used in order to minimize the switches commutation numbers and to have the two senses of the motor rotation. The output of this controller is represented by a Boolean variable K_T which indicates directly if the amplitude of the torque must be increased, maintained constant or decreased, respectively, when K_T is equal 1, 0 or -1. The goal of this controller is to maintain the torque variation $\Delta\Gamma$ in the bandwidth $[-\varepsilon_T, \varepsilon_T]$ chosen by the programmer of DTC algorithm. Indeed, this controller adjusts the torque variation generated by a comparator of electromagnetic torque reference (Γ^*) and the estimated torque ($\hat{\Gamma}$).

$$\Delta\Gamma = \Gamma^* - \hat{\Gamma} \quad (16)$$

3.3. Switching table for controlling flux and torque

According to the signal generated by the hysteresis controller of stator flux and electromagnetic torque presented in figure 3 and 5, respectively; just one voltage vector can be selected to adjust the torque and flux. The choice of this vector depends on the outputs of the torque and flux controller and the position of the stator flux vector, as shown in table 1.

K_Φ	K_T	θ_1	θ_2	θ_3	θ_4	θ_5	θ_6
1	1	V ₂	V ₃	V ₄	V ₅	V ₆	V ₁
	0	V ₇	V ₀	V ₇	V ₀	V ₇	V ₀
	-1	V ₆	V ₁	V ₂	V ₃	V ₄	V ₅
0	1	V ₃	V ₄	V ₅	V ₆	V ₁	V ₂
	0	V ₀	V ₇	V ₀	V ₇	V ₀	V ₇
	-1	V ₅	V ₆	V ₁	V ₂	V ₃	V ₄

Table 1. Takahashi and Noguchi switching table

3.4. Torque and flux estimator

In this chapter, two estimators of torque and stator flux will be presented.

3.4.1. Classical Torque and Flux Estimator (CTFE)

The figure 2 shows that the torque and stator flux can be estimated by measuring the mechanical position, stator voltages and currents. Indeed, the stator flux is estimated by using equations 11, 12 and 13. Whereas, the torque is estimated by using equation 17:

$$\hat{\Gamma} = \frac{3}{2}P[\Phi_{s\alpha}I_{s\beta} - \Phi_{s\beta}I_{s\alpha}] \quad (17)$$

Note that the stator voltages used in this estimator can be measured directly by mean of two or three sensors, or indirectly by combining the measured DC bus voltage and the transistor states (C_{s1}, C_{s3}, C_{s5}) of the VSI.

$$\begin{bmatrix} V_{s\alpha} \\ V_{s\beta} \end{bmatrix} = U_{dc} \sqrt{\frac{2}{3}} \begin{bmatrix} 1 & -\frac{1}{2} & -\frac{1}{2} \\ 0 & 1 & 1 \end{bmatrix} \begin{bmatrix} C_{s1} \\ C_{s3} \\ C_{s5} \end{bmatrix} \quad (18)$$

C_{s1} , C_{s3} and C_{s5} are the switching commands of each VSI leg and they are complementary. For the first leg (transistors S_1 and S_4), C_{s1} is 1 if the upper switch (S_1) is commanded to be closed and 0 if the lower one (S_4) is commanded to be closed first.

The drawbacks of this estimation technique are: In addition to stator current sensors, at least one voltage sensor is necessary. In addition, the estimated torque and stator flux dependent to the stator resistance.

3.4.2. Robust Torque and Flux Estimator (RTFE)

In order to estimate stator flux and electromagnetic torque with this estimator, just current components and rotor position are measured without measuring stator voltages directly or by using transistor states and DC bus voltage sensor. The bloc diagram of this estimation technique is shown in figure 6.

The advantages of this NTFE are: Any stator voltage sensor is necessary to estimate stator flux or electromagnetic torque and the estimated stator flux and electromagnetic torque are independent to the stator resistance variations, which can improve the performances of the drive and reduce the cost of this equipment.

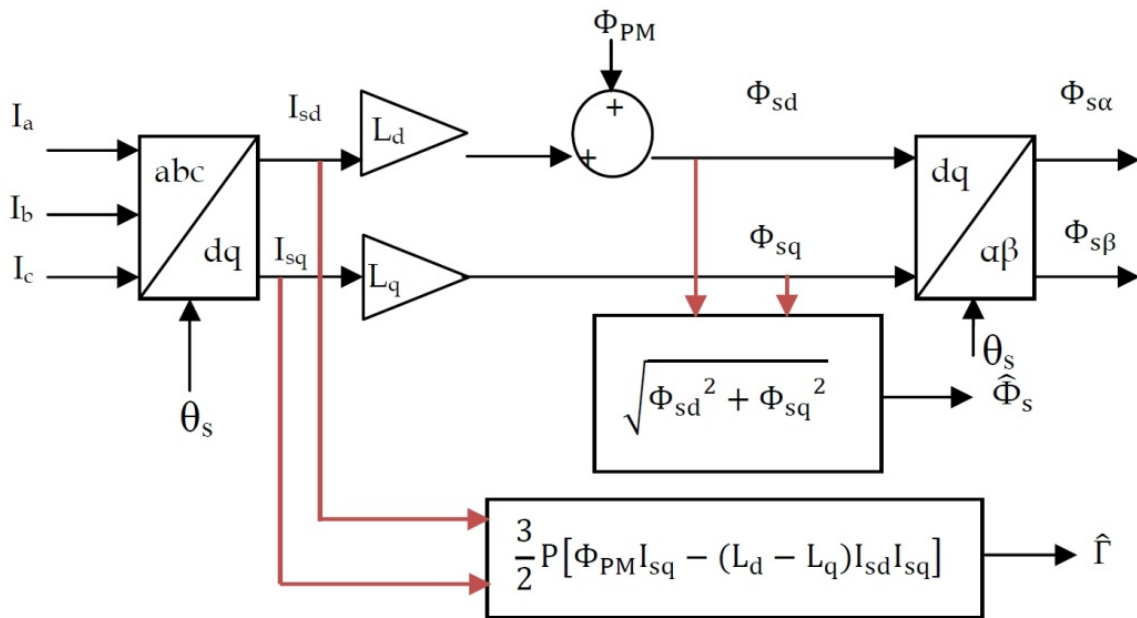


Figure 6. Robust Torque and Flux Estimator structure

3.5. Speed PI controller synthesis

The speed closed loop with the PI controller is presented by the bloc diagram in Figure 7. To eliminate the zero effect due to corrector, the compensation method is used to the corrector synthesis. In this case the regulator parameters are given by the relationships:

$$k_p = \frac{J}{K_T \cdot \tau_w} \text{ and } k_i = \frac{J}{K_T \cdot \tau_w} \text{ where } \tau_w = 0.1 \text{ second}$$

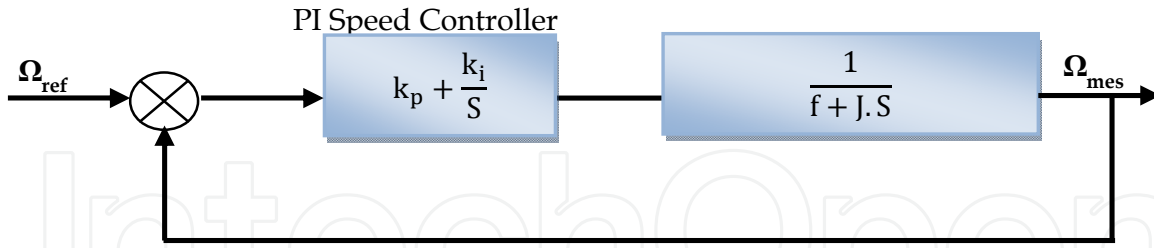


Figure 7. Closed loop PI speed controller

3.6. Simulation results

The PMSM parameters used in this simulation are shown in table II. These parameters will be used in all the simulations of this chapter.

Rated output power (Watt)	Rated phase voltage (Volt)	Magnetic flux linkage (Wb)
500	190	0.052
Rated torque (Nm)	Rated speed (r/min)	Maximum speed (r/min)
0.8	1000	6000
d-axis inductance (mH)	q-axis inductance (mH)	Inertia (Kg.m ²)
3.3	3.3	0.003573
Poles	Stator resistance (Ω)	friction coefficient (Nm.s/rd)
3	1.59	0.00047

Table 2. PMSM parameters

The models of the PMSM, VSI and basic DTC algorithm are developed in Matlab/Simulink in order to examine the complete behaviour of the basic DTC. The sampling period has been chosen equal to 50 μs (20 KHz) for basic DTC. Various tests have been carried out in order to investigate the drive performance and to characterize the steady-state and transient behavior.

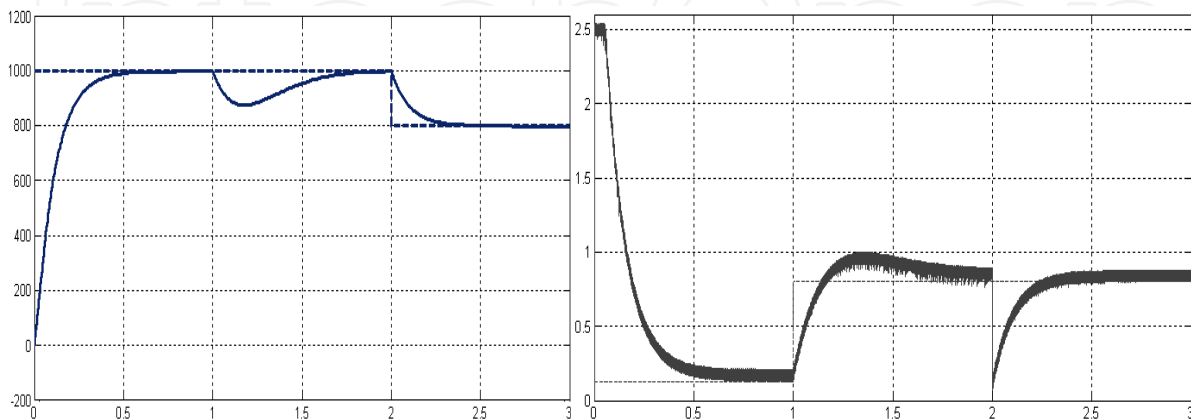


Figure 8. Mechanical speed (on the left) and electromagnetic torque (on the right) tracking performance under load variations in case of basic DTC

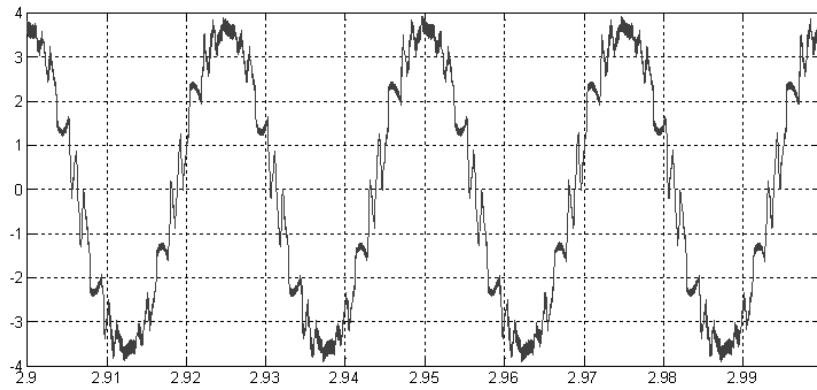


Figure 9. Stator current waveform at 800 rpm with nominal load under basic DTC

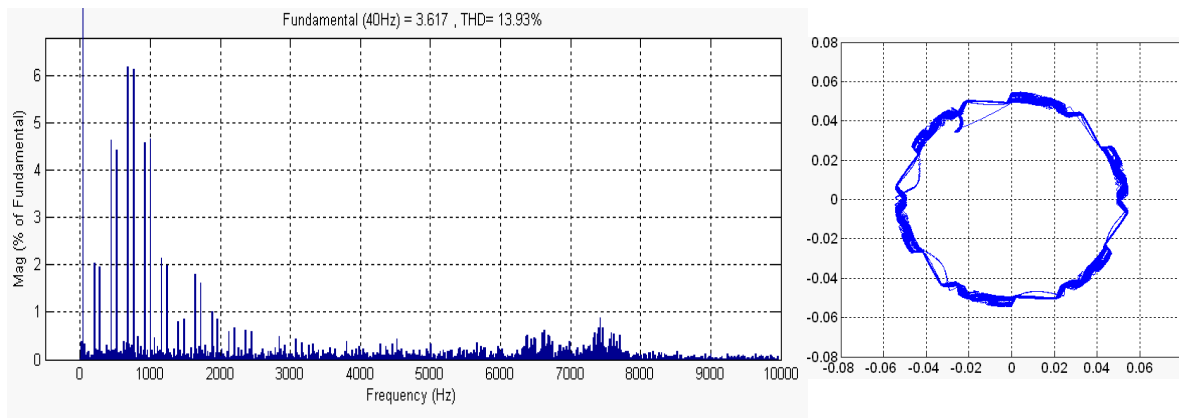


Figure 10. Stator current spectrum at 800 rpm with nominal load (on the left) and Stator flux in (α, β) axes under load variations (on the right) in case of basic DTC

4. Fuzzy direct torque control for PMSM

4.1. FDTC strategy

Figure 11 shows the complete FDTC structure which combines FDTC and PI-Fuzzy speed controller. Indeed, the switching table used in basic DTC and the hysteresis controllers are replaced by a fuzzy switching table, whose inputs are electromagnetic torque and stator flux errors denoted respectively $\Delta\Gamma$ and $\Delta\Phi_s$, and the argument θ_s of the stator flux (should remain between $\pm\pi$). Whereas its outputs are the states of the VSI switches. In other hand, the classical speed PI corrector is replaced by a PI-Fuzzy speed controller in order to improve the dynamic performance of the DTC.

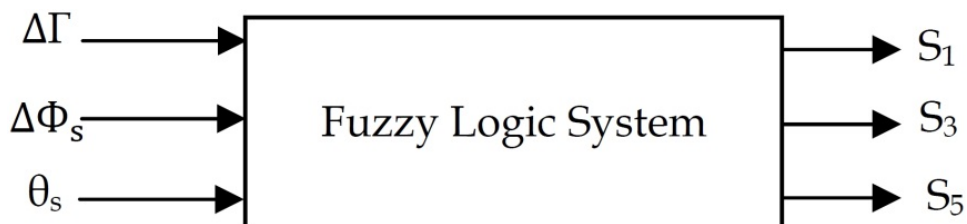


Figure 11. Fuzzy logic switching table used in FDTC

Figure 12 shows the design of this fuzzy logic system in Matlab/Simulink and also the configuration of its inputs and outputs as membership functions.

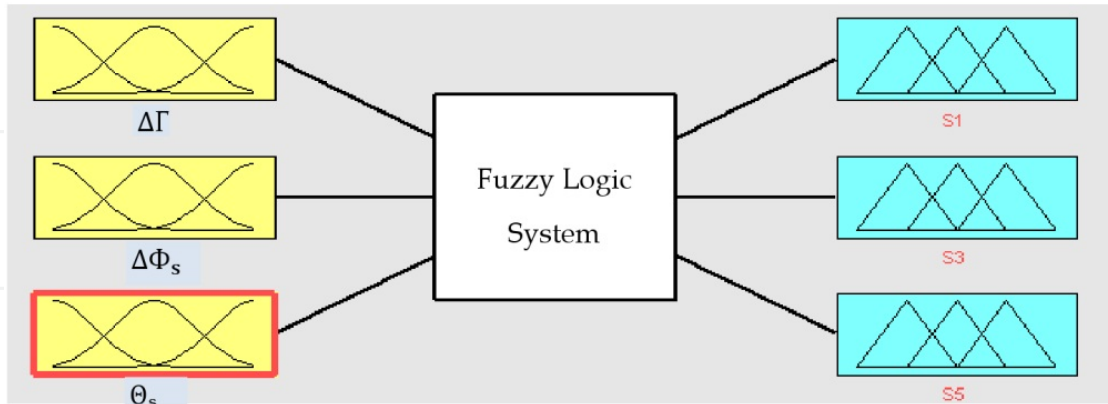


Figure 12. Matlab/Simulink design of the fuzzy logic switching table used in FDC

4.2. Inputs fuzzification and outputs defuzzification

In order to examine the fuzzy logic contribution to DTC, the choice of the membership functions number for the fuzzification of flux and torque errors has been repeated in this part, i.e two membership functions for $\Delta\Phi_s$, because a two level hysteresis controller was utilized to control the stator flux in basic DTC. Whereas three membership functions for the fuzzification of $\Delta\Gamma$ because a three level hysteresis controller was used to adjust the torque.

4.2.1. Stator flux error fuzzification

Two trapezoidal membership functions are selected to fuzzify the stator flux error, so the following two fuzzy sets are used, N signify Negative and P for Positive. The parameters of these two functions are indicated in figure 13.

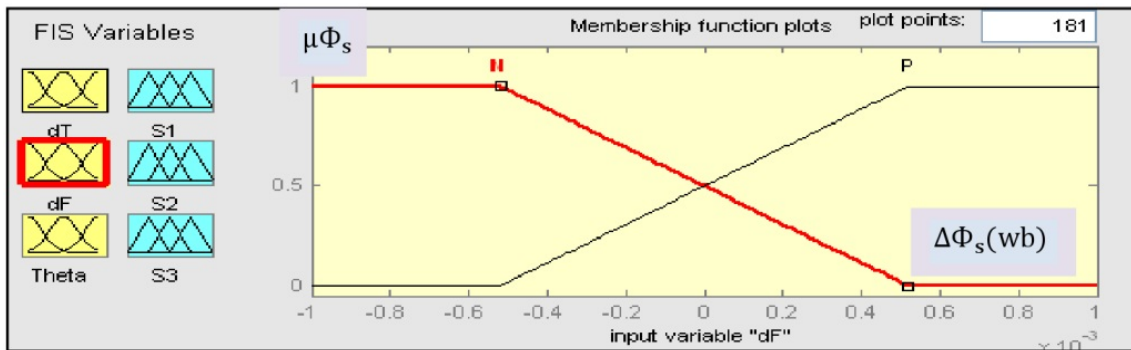


Figure 13. Membership functions for stator flux error

4.2.2. Electromagnetic torque error fuzzification

Three trapezoidal membership functions are selected to fuzzify the torque error as shown in figure 14, so the following three fuzzy sets are used, N signify Negative, EZ for Zero and P for Positive.

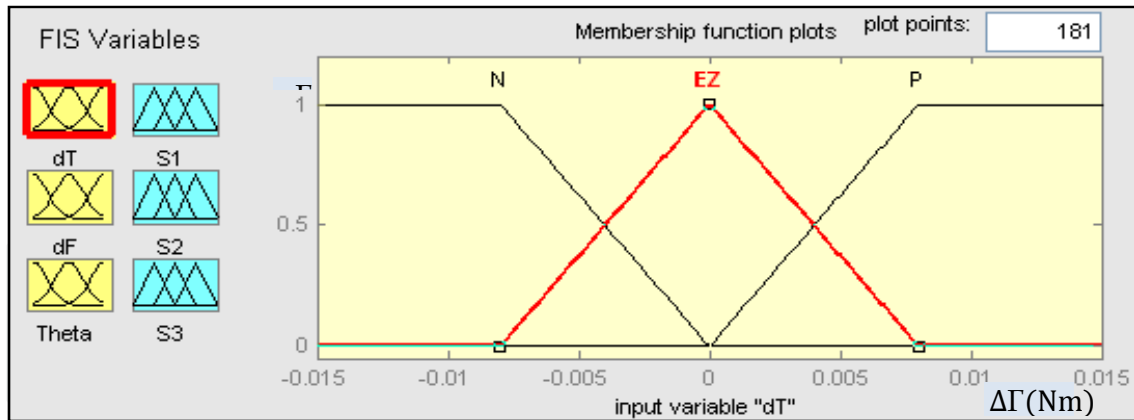


Figure 14. Membership functions for electromagnetic torque error

4.2.3. Stator flux angle fuzzification

The flux angle has a universe of discourse equal 2π radians, as shown in figure 15. It is divided into six zones or sectors in order to be equivalent to that of the basic DTC. “theta_i” means sector i, i.e. “theta₁” means sector 1 (θ_1) and so on.

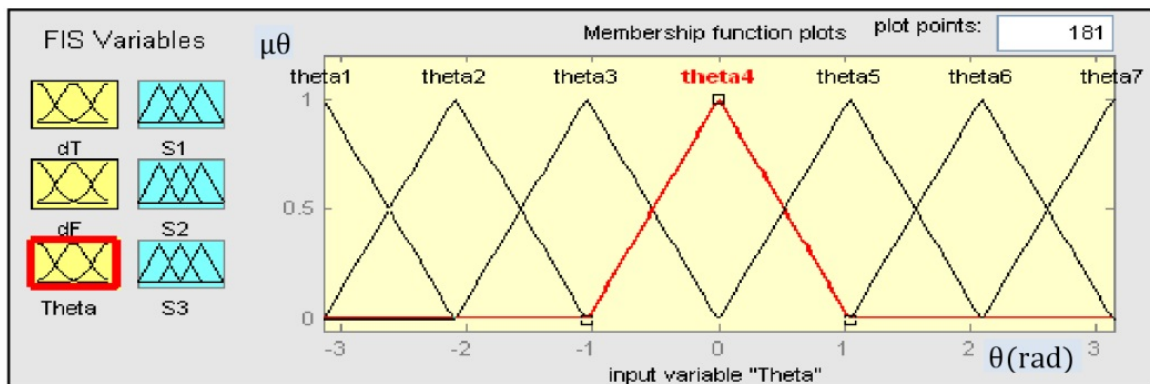


Figure 15. Membership functions for stator flux position

4.2.4. State switches defuzzification

The sole output control variable of fuzzy logic system is the inverter switching states S_1 , S_3 and S_5 or the selected voltage vector. Figure 16, illustrates the suggested output fuzzy set as singletons. Indeed, the choice of the stator voltage vector is based on the rules indicated in table 3. Each control rule can be described using the state variables $\Delta\Phi$, $\Delta\Gamma$ and θ_s and the control variables. The i th rule R_i can be written as:

$$R_i : \text{if } \Delta\Phi \text{ is } A_i, \Delta\Gamma \text{ is } B_i \text{ and } \theta_s \text{ is } C_i \text{ then } S_1 \text{ is } a, S_3 \text{ is } b \text{ and } S_5 \text{ is } c$$

Where a , b and c are a boolean variable. A_i , B_i and C_i denote the fuzzy set of the variables $\Delta\Phi$, $\Delta\Gamma$ and θ_s , respectively. whereas R_i is the control rule number i .

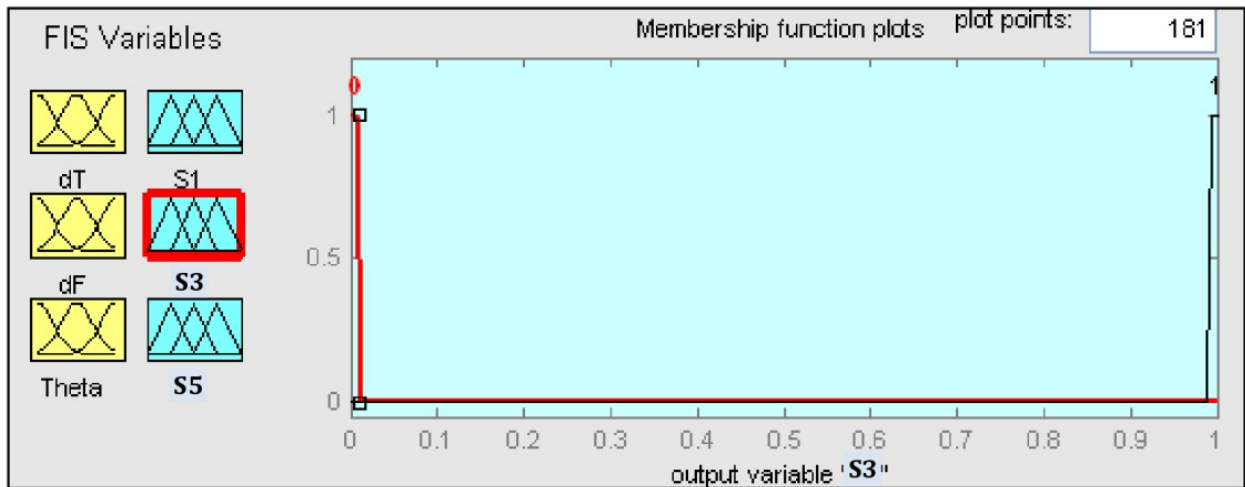


Figure 16. Membership functions for state switches as singletons

4.3. Fuzzy logic switcher rules

The most important part of designing the fuzzy controller (fuzzy logic system) is to design the rule base, because it governs the behaviour of fuzzy controller and stores the expert knowledge on how to control the plant. The fuzzy associative memory of Mamdani rule base model to develop DTFC is as shown in Table 3.

θ_1, θ_7			θ_2			θ_3		
$\Delta\Gamma \backslash \Delta\Phi$	P	N	$\Delta\Gamma \backslash \Delta\Phi$	P	N	$\Delta\Gamma \backslash \Delta\Phi$	P	N
P	V ₅	V ₆	P	V ₆	V ₁	P	V ₁	V ₂
Z	V ₀	V ₇	Z	V ₇	V ₀	Z	V ₀	V ₇
θ_4			θ_5			θ_6		
$\Delta\Gamma \backslash \Delta\Phi$	P	N	$\Delta\Gamma \backslash \Delta\Phi$	P	N	$\Delta\Gamma \backslash \Delta\Phi$	P	N
P	V ₂	V ₃	P	V ₃	V ₄	P	V ₄	V ₅
Z	V ₇	V ₀	Z	V ₀	V ₇	Z	V ₇	V ₀

Table 3. Fuzzy logic switcher rules

4.4. PI-Fuzzy speed controller synthesis

The speed closed loop with the PI-Fuzzy controller structure is shown in Figure 17. The inputs of this FLC are the normalized values of the speed error denoted “e” and its rate of change denoted “de” that should remain between ± 1 . Wherefore, two scaling factors (K_{ne} and $K_{\Delta ne}$) are used to normalize the actual speed error and its rate of change. The output of the controller is the normalized change of the motor torque command which generates the actual value of the motor torque demand when it’s multiplied by a third scaling factor (K_{nc}).

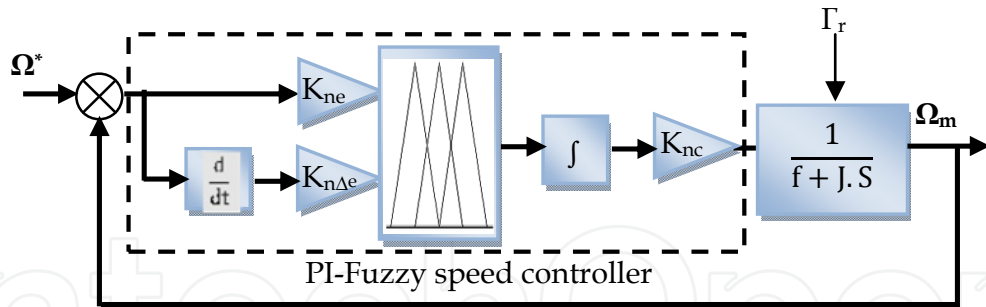


Figure 17. Closed loop PI-Fuzzy speed controller

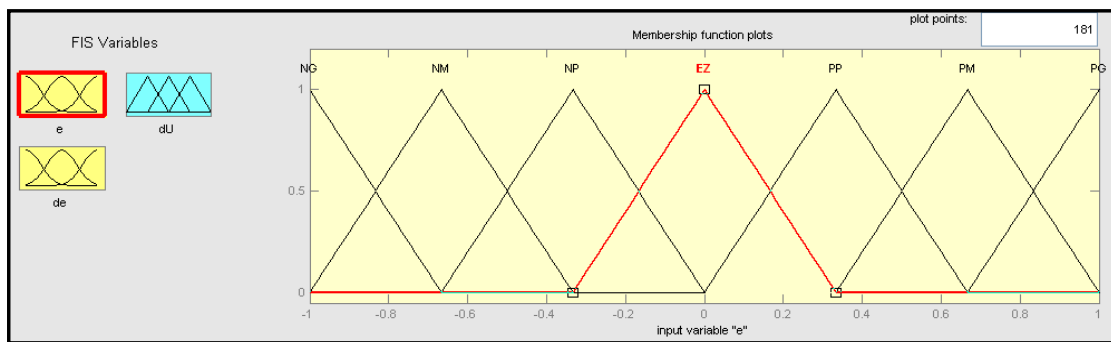


Figure 18. Membership functions for speed error

The membership functions used, in this chapter, for the inputs and the output are the same, as shown in figure 18. Where, the following fuzzy sets used in these membership functions: NG is negative big, NM is negative medium, NP is negative small, EZ is equal zero, PP is positive small, PM is positive medium and PG is positive big.

From the speed behavior analysis, the table 4 has been developed to obtain a good performance in the speed closed loop. Whereas, from the membership functions of inputs and the output, and the rules presented in this table, the FLC elaborates the electromagnetic torque reference to be developed by the PMSM.

e\Δe	NG	NM	NP	EZ	PP	PM	PG
PG	EZ	PP	PM	PG	PG	PG	PG
PM	NP	EZ	PP	PM	PG	PG	PG
PP	NM	NP	EZ	PP	PM	PG	PG
EZ	NG	NM	NP	EZ	PP	PM	PG
NP	NG	NG	NM	NP	EZ	PP	PM
NM	NG	NG	NG	NM	NP	EZ	PP
NG	NG	NG	NG	NG	NM	NP	EZ

Table 4. PI-Fuzzy speed controller rules

4.5. Simulation results

The sampling period has been chosen equal to 100 μ s (10 KHz) for FDTC; in order to compare this strategy with basic DTC; despite the fact that the sampling time used to simulate DTC is less than that used in case of FDTC.

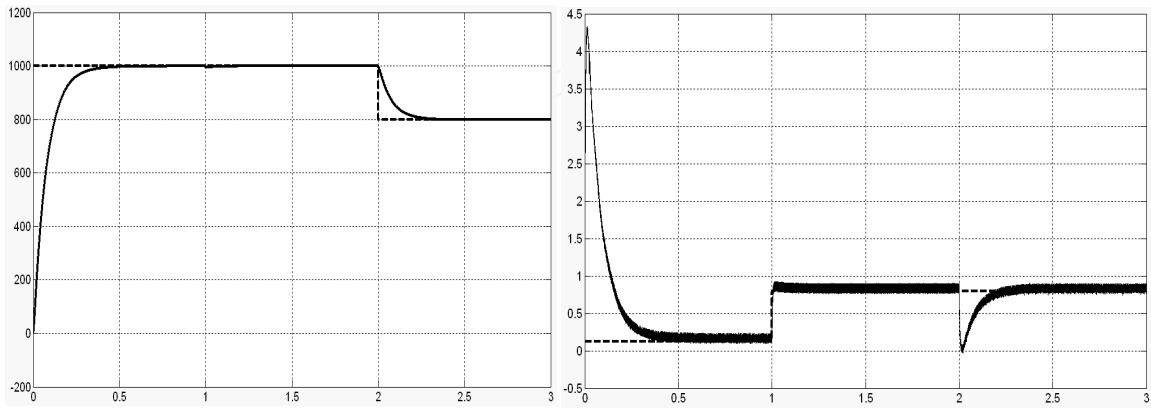


Figure 19. Mechanical speed (on the left) and electromagnetic torque (on the right) tracking performance under load variations in case of FDTC

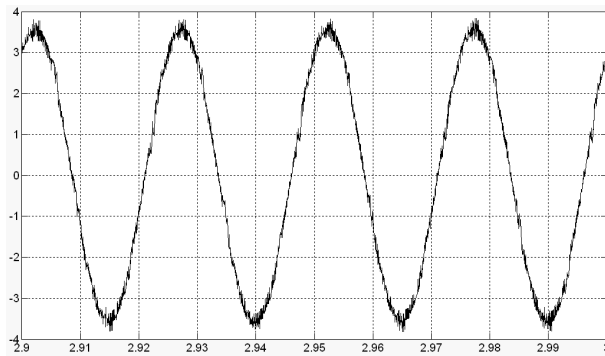


Figure 20. Stator current waveform at 800 rpm with nominal load under FDTC

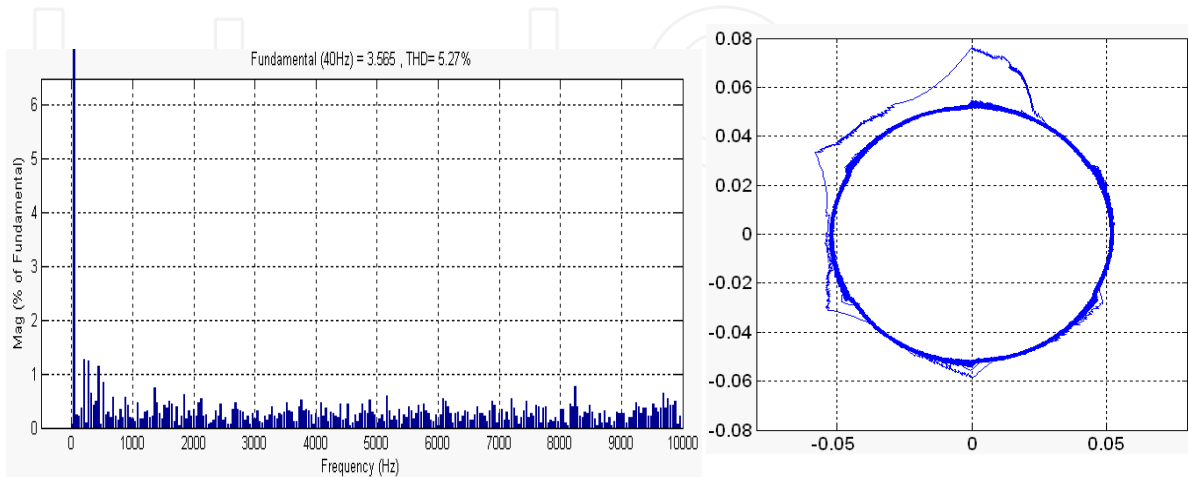


Figure 21. Stator current spectrum at 800 rpm with nominal load (on the left) and Stator flux in (α, β) axes under load variations (on the right) in case of FDTC

5. Direct Torque Control with Space Vector Modulation for PMSM

Figure 22 shows the DTC with SVM scheme for PMSM drive, this technique is a solution to overcome the drawbacks of the basic DTC by using the same torque and flux estimators and the same speed PI controller. In this modified DTC, torque and flux hysteresis controllers and the switching table used in basic DTC are replaced by a PI torque controller and a predictive calculator of vector voltage reference to be applied to stator coils of the PMSM.

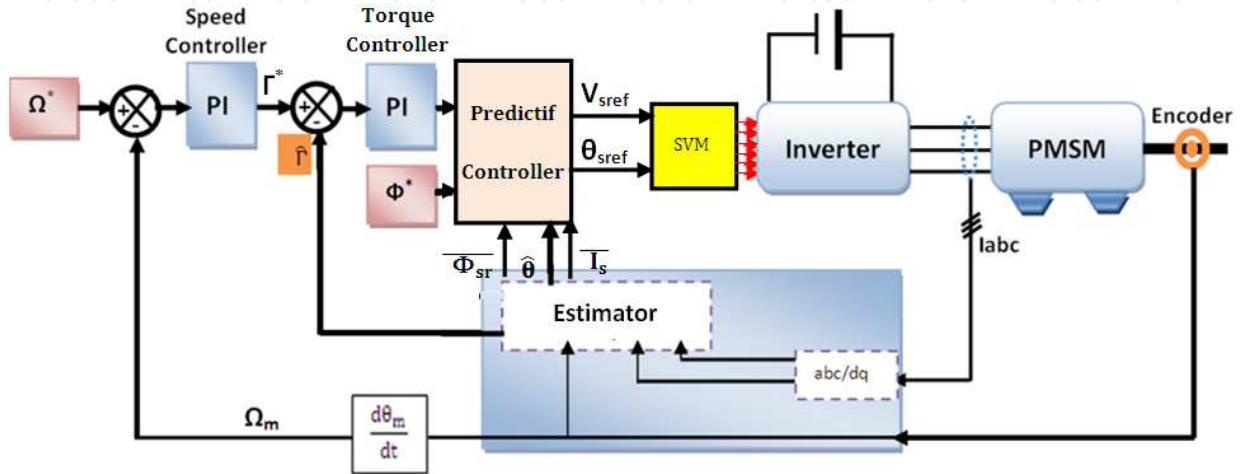


Figure 22. DTC-SVM scheme for PMSM drive

In the proposed scheme of DTC-SVM with speed loop control, shown in this figure, after correction of the mechanical speed through a PI controller, the torque PI controller delivers V_{sq} voltage to the predictive controller and also receives, more the reference amplitude of stator flux $\Phi^* = \Phi_{PM}$, information from the estimator namely, the position of the actual stator flux, estimated flux vector and measured current vector, where:

$$\overline{\Phi_s} = \Phi_{s\alpha} + j\Phi_{s\beta} \text{ and } \overline{I_s} = i_{s\alpha} + ji_{s\beta}$$

After calculation, the predictive controller determinates the polar coordinates of stator voltage command vector $\overline{V_{sref}} = [V_{sref}, \theta_{sref}]$ for space vector modulator, which finally generates the pulses S_1, S_3 and S_5 to control the VSI.

5.1. Torque and flux control by means of SVM

The electromagnetic torque of the PMSM can be expressed as:

$$\Gamma_{em} = \frac{3}{2} P \frac{\Phi_{sr}}{L_d L_q} \left[\Phi_{PM} L_q \sin \delta + \frac{1}{2} \Phi_{sr} (L_d - L_q) \sin \delta \right] \quad (19)$$

Where δ is the angle between the stator and rotor flux linkage (or the torque angle).

Above equation consist of two terms, the first is the excitation torque, which is produced by permanent magnet flux and the second term is the reluctance torque.

In the case where $L_d = L_q = L$, the expression of electromagnetic torque becomes:

$$\Gamma_{em} = \frac{3}{2} P \frac{\Phi_{sr}}{L} \Phi_{PM} \sin \delta \tag{20}$$

Under the condition of constant stator flux amplitude Φ_{sr} , by differentiating equation 20 with respect to time, the rate of increasing of torque at $t=0$ can be obtained in equation 21.

$$\frac{d\Gamma}{dt} = \left(\frac{3}{2} P \frac{\Phi_{sr}}{L} \Phi_{PM} \cos \delta \right) \frac{d\delta}{dt} \tag{21}$$

From equations 20 and 21, it can be seen that for constant stator flux amplitude Φ_{sr} and flux produced by Permanent Magnets (PM) Φ_{PM} , the electromagnetic torque can be changed by control of the torque angle; quick dynamic response can be achieved by changing this angle as quickly as possible, this is the basis of DTC for PMSM (Tang et al., 2003). This is the angle between the stator and rotor flux linkage, when the stator resistance is neglected. The torque angle δ , in turn, can be changed by changing position of stator flux vector in respect to PM vector using the actual voltage vector supplied by PWM inverter.

When the PMSM drive, we distinguish between two cases:

- Steady state: the angle δ is constant and its value is the load torque of the machine, while the stator flux and rotor rotate at the same speed is the synchronous speed.
- The transient state, the angle δ is variable then the stator and rotor flux rotate at different speeds (see figure 23).

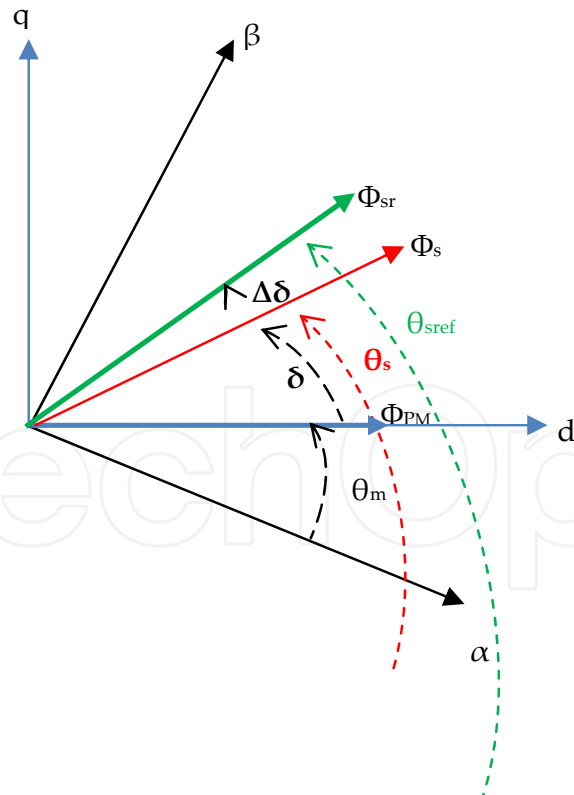


Figure 23. Vector diagram of illustrating torque and flux control conditions

The change of the angle δ is done by varying the position of the stator flux vector relative to the rotor flux vector with the vector V_{sref} provided by the predictive controller to the power

of the SVM. The figure 23 above shows the evolution of the stator flux vector at the beginning and the end of a period vector modulation. At the beginning, stator flux vector is at the position δ with an amplitude Φ_s , it's at this moment that the predictive controller calculated the variation $\Delta\delta$ of the stator flux angle, it's also at this same moment that the space vector modulator receives the new position and amplitude of the voltage vector that must be achieved at the end of the modulation period. Of course, this vector will allow the stator flux to transit to the location as defined by the predictive controller to adjust the torque fluctuations, and this by calculating the time of application of the adjacent vectors V_1 , V_2 and V_0 as well as their sequence that depends on the symmetry of the modulation vector.

The internal structure of the predictive torque and flux controller is shown in figure 24. So the average change $\Delta\delta$ of the angle δ is expressed as:

$$\Delta\delta = T_s \frac{d}{dt} \left[\text{Arcsin} \left(\frac{\Phi_{sr}}{L_q I_{sq}} \right) \right] \quad (22)$$

where: T_s is the sampling time.

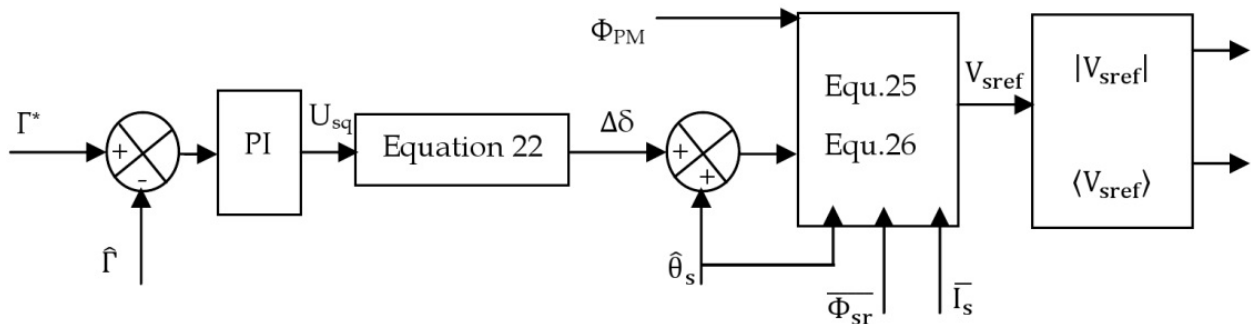


Figure 24. Internal structure of predictive controller used in DTC-SVM

From equation 22, the relation between error of torque and increment of load angle $\Delta\delta$ is non linear. In order to generate the load angle increment required to minimize the instantaneous error between reference and actual estimated torque; a PI controller has been applied as indicated in figure 24. The step change $\Delta\delta$ that corresponds to the torque error is added to the current position $\hat{\theta}_s$ of the stator flux vector to determine the new position of this vector at the next simple time.

The module and argument of the reference stator voltage vector is calculated by the following equations, based on stator resistance R_s , $\Delta\delta$ signal and actual stator flux argument:

$$|V_{sref}| = \sqrt{V_{s\alpha-ref}^2 + V_{s\beta-ref}^2} \quad (23)$$

$$\langle V_{sref} \rangle = \arctan \left(\frac{V_{s\beta-ref}}{V_{s\alpha-ref}} \right) \# \quad (24)$$

Where:

$$V_{s\alpha-ref} = \frac{\Phi_{sr} \cos(\hat{\theta}_s + \Delta\delta) - \Phi_s \cos \hat{\theta}_s}{T_s} + R_s \cdot I_{s\alpha} \quad (25)$$

$$V_{s\beta-ref} = \frac{\Phi_{sr} \sin(\hat{\theta}_s + \Delta\delta) - \Phi_s \sin \hat{\theta}_s}{T_s} + R_s \cdot I_{s\beta} \tag{26}$$

The figure 25 shows the application sequence of the two adjacent vectors and zero vector in the first sector of the vector V_{sref} . Indeed, after the vector modulation algorithm computation times T_1 , T_2 and T_0 successively apply the voltage vectors V_1 , V_2 and V_0 , we choose the symmetry in the schematic figure 25 of dividing each modulation period T_s into two sequences and transistor control of the upper arms of the VSI, in the second half of the period are an image of themselves in relation to the vertical axis passing through the point $T_s/2$.

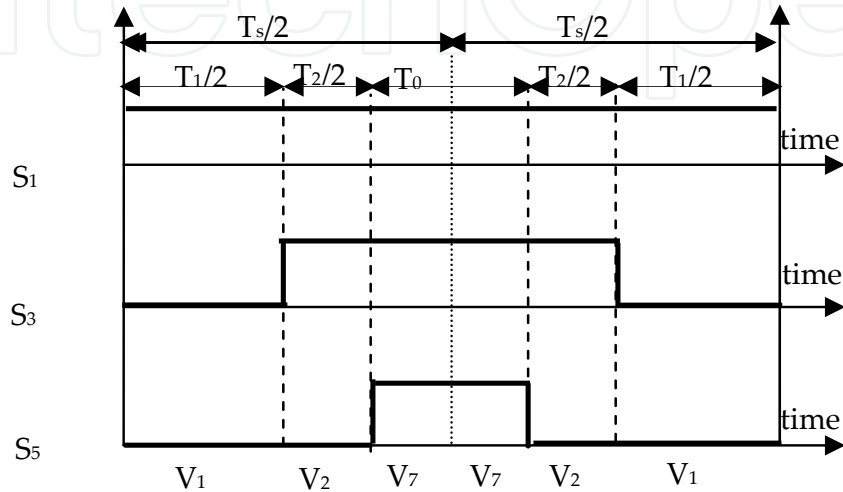


Figure 25. Time sequences and applications of adjacent vectors in the first sector

So to have a fast transit of stator flux vector, very low flux ripple and fast torque response, the space vector modulator generates a voltage vector V_{sref} governed by the following law:

$$V_{sref} = \frac{1}{T_s} \left[\left(\frac{T_1}{2} V_1 + \frac{T_2}{2} V_2 + \frac{T_0}{2} V_0 \right) + \left(\frac{T_0}{2} V_0 + \frac{T_2}{2} V_2 + \frac{T_1}{2} V_1 \right) \right] \tag{27}$$

So at each modulation period and in this case, the sequence of adjacent vectors in the first sector is applied (V_1 - V_2 - V_7 - V_7 - V_2 - V_1) respectively during the time $\left(\frac{T_1}{2}, \frac{T_2}{2}, \frac{T_0}{2}, \frac{T_0}{2}, \frac{T_2}{2}, \frac{T_1}{2} \right)$ to rebuild the better the rotating vector.

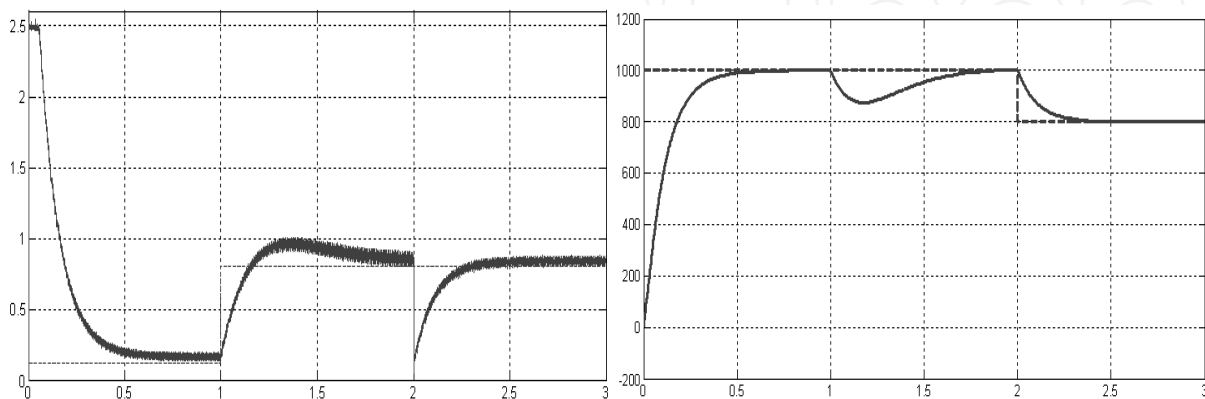


Figure 26. Stator current spectrum at 800 rpm with nominal load (on the left) and Stator flux in (α, β) axes under load variations (on the right) in case of DTC-SVM

5.2. Simulation results

The sampling period has been chosen equal to $100 \mu\text{s}$ (10 KHz) for DTC-SVM; in order to compare this strategy with basic DTC; despite the fact that the sampling time used to simulate DTC is less than that used in case of DTC-SVM. Whereas, the sampling frequencies used to simulate FDTC and DTC-SVM are equal; so as to compare these two techniques in the same conditions.

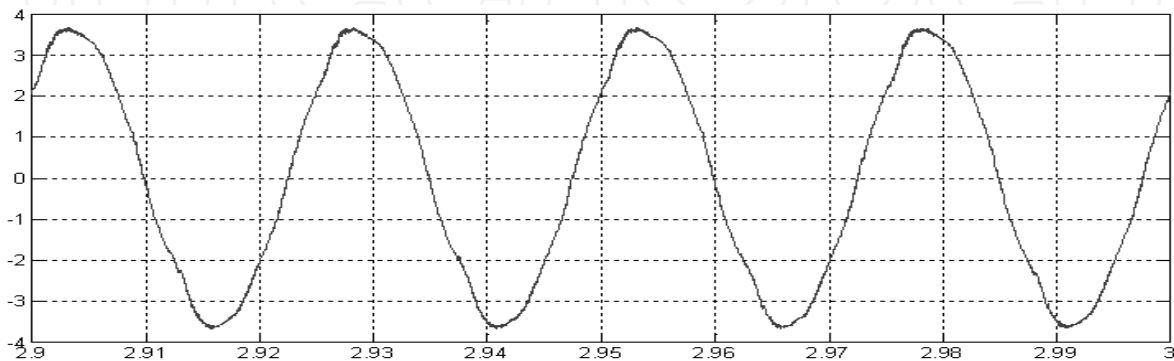


Figure 27. Stator current waveform at 800 rpm with nominal load under DTC-SVM

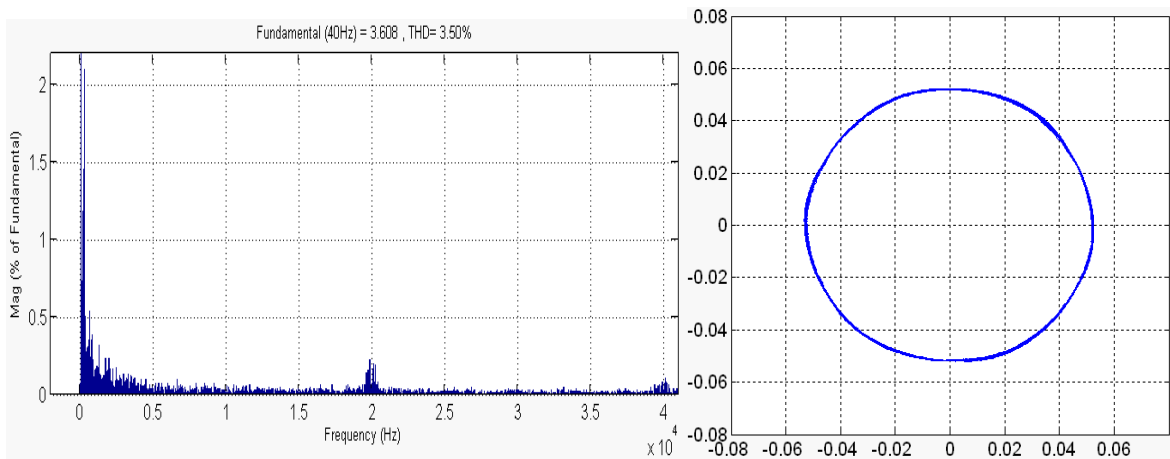


Figure 28. Stator current spectrum at 800 rpm with nominal load (on the left) and Stator flux in (α, β) axes under load variations (on the right) in case of DTC-SVM

6. Direct Torque Control with Sinusoidal Pulse with Modulation for PMSM

DTC-SPWM for PMSM is based on the same algorithm used in DTC-SVM already presented in figure 22, but instead of using SVM pulses generator, a simple and fast SPWM pulses generator is investigated to control the VSI. Indeed, after transformation of $V_{s\alpha-ref}$ and $V_{s\beta-ref}$ produced by the predictive controller (from the stator flux reference frame $(\alpha-\beta)$ to the $(a-b-c)$ frame). These three signals, used as reference signals, will be compared with a triangular signal (figure 29); then the inverter is controlled by the SPWM.

In this proposed technique, the same flux and torque estimators and the predictive torque and flux controller as for the DTC-SVM are still used. Instead of the SVM generator, a SPWM technique is used to determine reference stator flux linkage vector. It is seen that the proposed scheme retains almost all the advantages of the DTC-SVM, such as no current control loop, constant switching frequency, low torque and flux ripple, etc. But, the main advantage of the DTC-SPWM is the simple algorithm of PWM (SPWM) used to control the VSI. Of course, the SVM algorithm needs more calculation time than SPWM and the same advantages of DTC-SVM will be obtained by using DTC-SPWM. Whatever is the load torque and speed variation, SPWM guarantees a constant switching frequency, which greatly improves the flux and torque ripples.

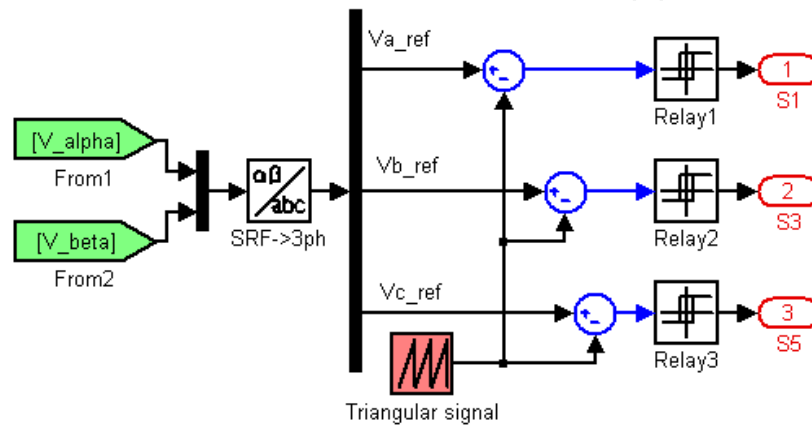


Figure 29. Sinusoidal PWM pulses generator scheme

6.1. Simulation results

The sampling period has been chosen equal to 100 μ s (10 KHz) for DTC-SVM; in order to compare this strategy with basic DTC; despite the fact that the sampling time used to simulate DTC is less than that used in case of DTC-SVM. Whereas, the sampling frequencies used to simulate FDTC and DTC-SVM are equal; so as to compare these two techniques in the same conditions.

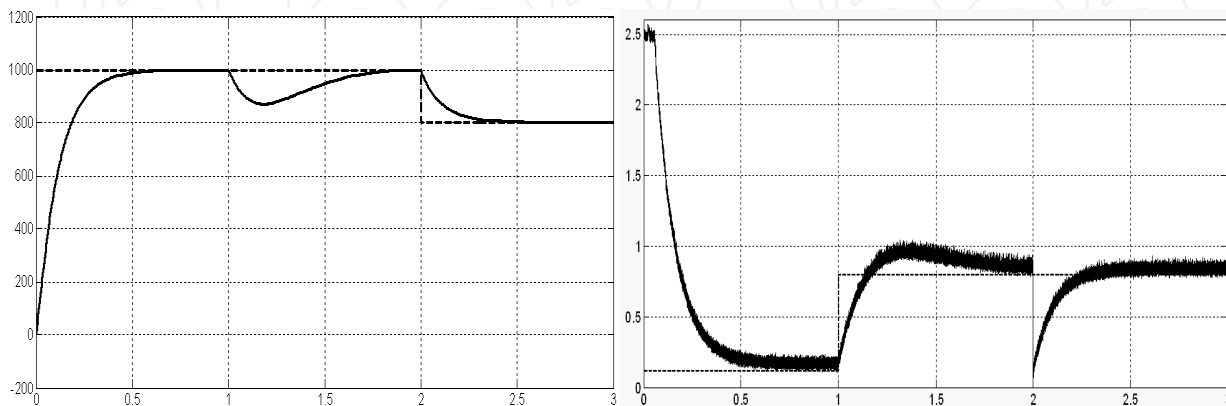


Figure 30. Stator current spectrum at 800 rpm with nominal load (on the left) and Stator flux in (α, β) axes under load variations (on the right) in case of DTC-SPWM

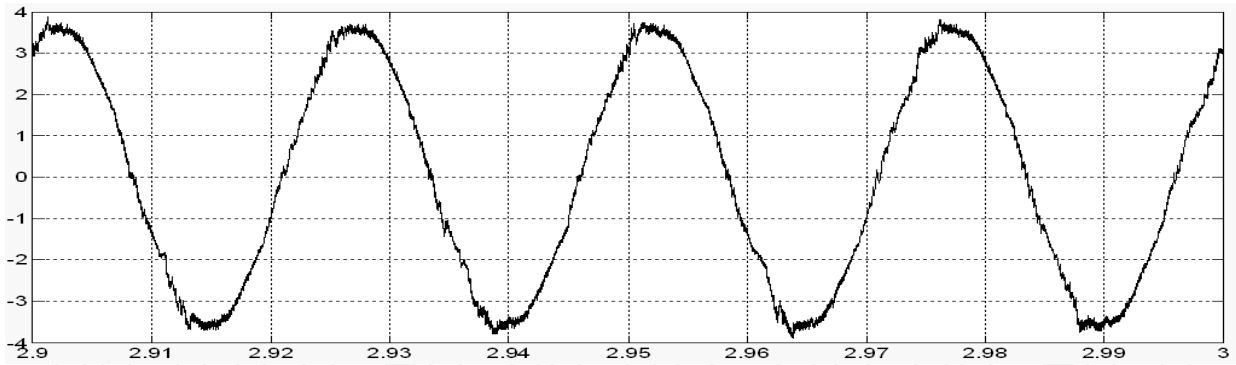


Figure 31. Stator current waveform at 800 rpm with nominal load under DTC-SPWM

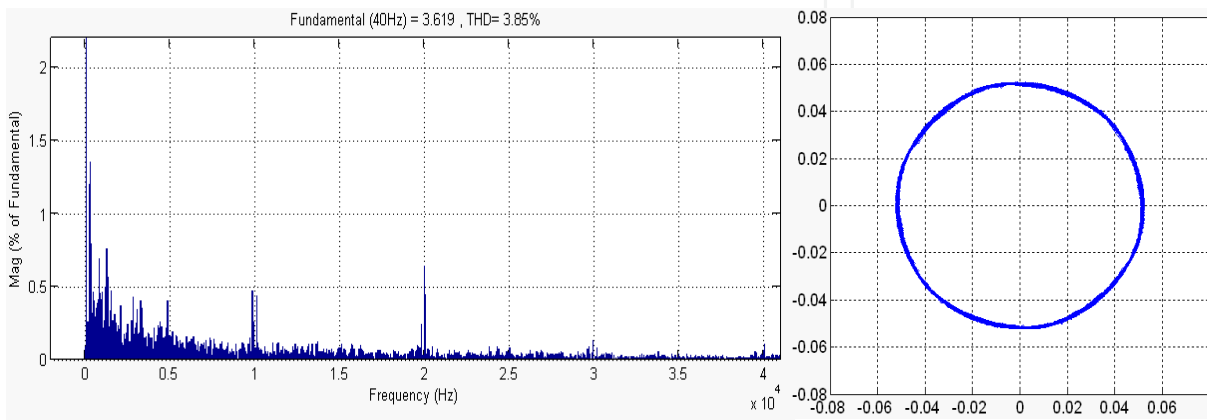


Figure 32. Stator current spectrum at 800 rpm with nominal load (on the left) and Stator flux in (α, β) axes under load variations (on the right) in case of DTC-SPWM

7. Comparison of DTC strategies

To verify and to compare the four DTC strategies proposed in this chapter, digital simulations have been carried out, by using the environment Matlab/Simulink, for the same PMSM parameters and conditions, except the sampling frequency utilized to simulate basic DTC which was taken equal to 20 KHz while for the FDTC, DTC-SVM and DTC-SPWM was taken equal to 10 KHz. Taking into consideration those conditions, the strategies' performances have been compared for both regimes dynamic and steady state.

Dynamic state: Figures 8, 26 and 30 shows that DTC, DTC-SVM and DTC-SPWM present the same speed and torque response time. Whereas, it's seen in figure 19 that torque and speed response time was greatly improved; at start time and at load torque or speed set-point variation. Indeed, speed FLC used in FDTC improves the dynamic state performances when compared to speed PI controller used in the other strategies.

Steady state: Figure 10 (on the left) show the spectral analysis of current presented in figure 10, it's seen that the Total Harmonic Distortion (THD) of the current waveform under basic DTC is 13.93 %. Whereas, figure 21 show that FDTC allows to decrease the THD value to 5.27 % with a variable switching frequency as indicated in the current spectral analysis. In addition, torque and stator flux ripple are reduced in case of FDTC in

comparison with basic DTC, and also the current quality was improved. Figure 28 (on the left) shows that the current THD under DTC-SVM is 3.5 %, which is smoother than that of basic DTC and FDTC. Also, it's seen that torque and flux ripples are greatly reduced under DTC-SVM when compared to DTC and FDTC (compare figures 26 and 28 with figures 8, 10, 19 and 21). Figure 32 shows that the THD of the current waveform under DTC-SPWM is 3.85%, which is almost the same as DTC-SVM, also DTC-SVM guarantees a constant switching frequency; as shown in figure 32 which allow to reduce torque and flux ripple as the same as DTC-SVM. Furthermore, the calculation time of the DTC-SPWM is much inferior to the DTC-SVM, this is because SPWM algorithm is very simple than SVM. Note that the SVM symmetry used in this work eliminates the harmonics which are around the uneven switching frequency (Chikh et al., 2011a). The same performances for DTC-SVM and DTC-SPWM can be obtained if an asymmetric SVM has been used instead of symmetrical SVM.

8. Effect of PMSM parameters variations and their compensation

This part is devoted to compare two speed controllers performances used in DTC under PMSM parameters variations. Also, a comparison between classical and novel torque and flux estimators has been developed in order to show their performances under PMSM parameters variations.

8.1. PI and FLC performances

Figure 33 shows the rotation speed and motor torque evolution for PMSM DTC strategy by using PI speed controller (green color) and speed FLC (red color). Indeed, the FLC has exhibited high performance in tracking the speed reference, as compared with speed PI controller. This figure confirms that the motor torque response with fuzzy controller is faster than PI controller during the start up regime and during a step change in load torque. The speed dynamic state imposes the motor torque response time because these two variables are regulated in cascade: the inner loop controls the motor electromagnetic torque and the outer loop regulates the motor rotation speed.

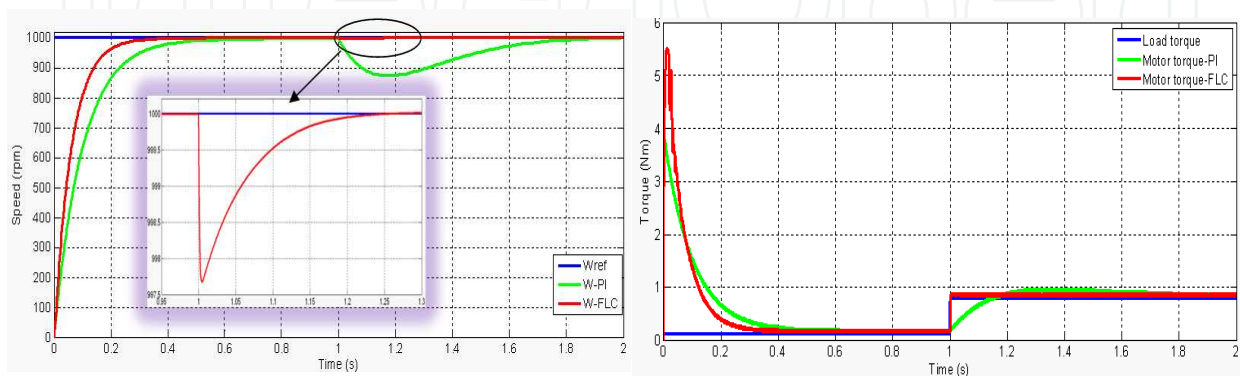


Figure 33. Rotation speed (on the left) and motor torque (on the right) performances under DTC for PMSM drive by using speed PI controller (green color) or speed FLC (red color)

8.2. Classical and novel estimators under stator resistance variation

The simulation results presented in this part shows the robustness of the classical and the novel flux and torque estimators, described at the beginning of this chapter, under stator resistance variation. Figure 34 shows the stator resistance variation applied to examine DTC for PMSM drive by using classical or novel estimator. In this case, the value of stator resistance was changed from the nominal value 1.59Ω to the double of this value 3.18Ω . Where, the reference stator flux and load torque are kept constant at 0.052 Wb and 0.8 Nm , respectively.

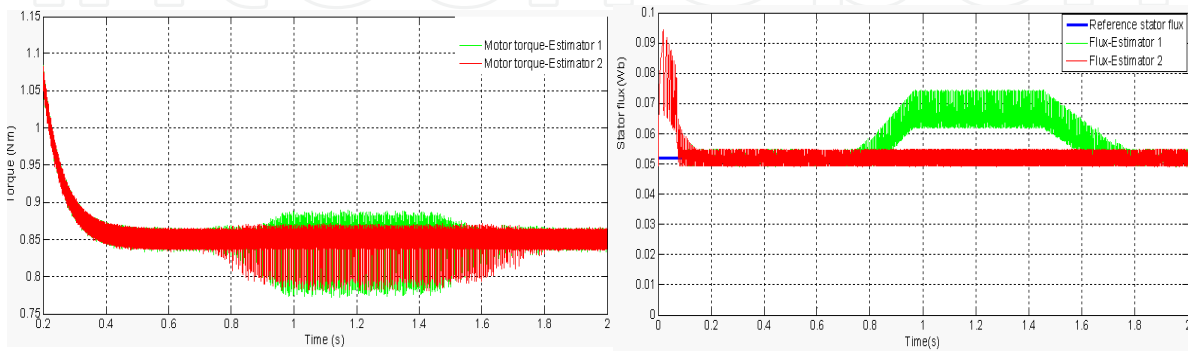


Figure 34. Stator resistance variation

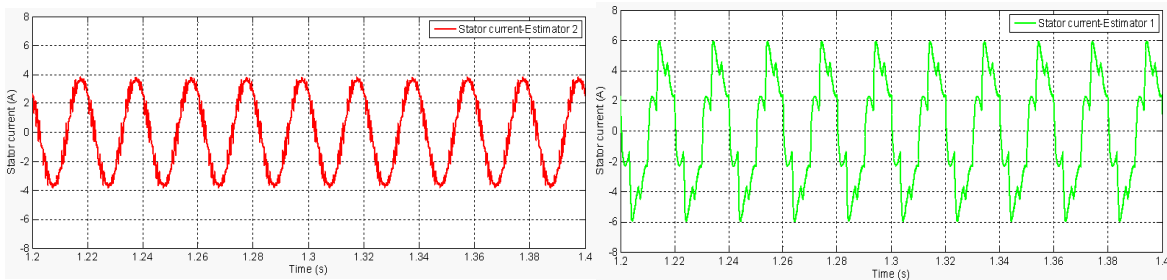


Figure 35. Motor torque (on the left) and stator flux (on the right) evolution by using classical estimator (green color) or by using novel estimator (red color)

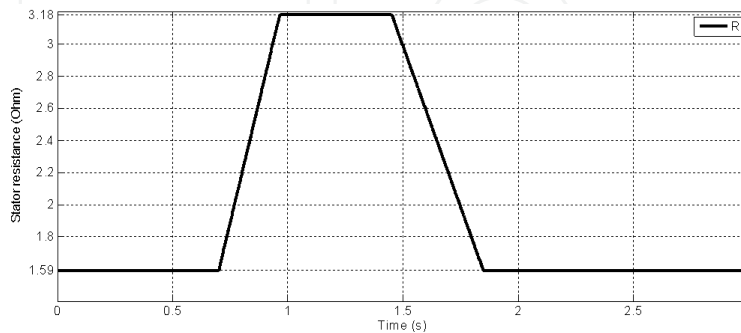


Figure 36. Stator current waveform in case of classical estimator (on the left) and novel estimator (on the right)

It's seen in figure 35 that the estimated stator flux was affected, when the stator resistance was changed at $t=0.75 \text{ s}$; when the stator flux was estimated by using classical estimator.

This figure shows that, in spite of stator resistance variation, the stator flux was maintained constant when it is estimated by the novel estimator, because this estimator does not depend on the stator resistance variation. This stator flux deviation is normal and forecasted because the estimated flux value by using classical estimator depends on the stator resistance. When the PMSM stator resistance varies; while this classical estimator still uses the nominal stator resistance to estimate the actual stator flux; the estimated stator flux differs significantly from the real stator flux.

As shown in figure 35, the torque and flux ripples are increased when stator resistance varies in case of classical estimator, because the stator flux deviation causes the DTC algorithm to select a wrong switching state, which can result in unstable operation of the PMSM. Indeed, figure 36 shows that the stator current waveform in case of the novel estimator presents a good THD than the current in case of classical estimator, this is due to the wrong selection of the switching state.

8.3. Classical and Robust estimators under PMSM parameters variation

The simulation results below present the DTC for PMSM performances in case of speed PI controller and Robust estimator, and speed FLC and this estimator under motor parameters variation, which are stator resistance, friction coefficient and motor inertia. Figure 37 (on the left) shows the variations, of these three parameters, applied to examine DTC robustness: the stator resistance was changed from the nominal value 1.59Ω to the double of this value 3.18Ω , the friction coefficient was changed from the nominal value $f=0.00047 \text{ Nm.s/rd}$ to $f1=100*f$ and the motor inertia was changed from the nominal value $J=0.003573 \text{ Kg.m}^2$ to $J1=100*J$.

It's seen in figure 37 (on the right) that the speed FLC allows to achieve a faster response and reject the perturbations (motor parameters variations), whereas the speed PI controller takes much time, in comparison with FLC, to reject these perturbations. Also, a faster motor torque response has been achieved with speed FLC compared to speed PI controller; as shown in figure 38 (on the left). Indeed, combining speed FLC and the novel estimator allow DTC for PMSM to reject stator resistance variation thanks to this estimator and reject motor inertia and friction coefficient thanks to speed FLC, which is shown in figure 38 (on the right).

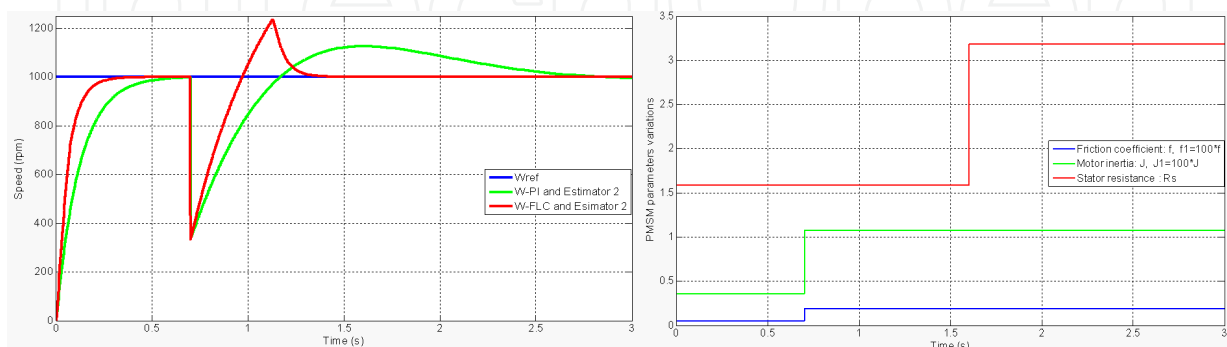


Figure 37. PMSM parameters variation (on the left) and rotation speed evolution (on the right) in case of DTC for PMSM drive using speed PI controller and novel estimator (green color), and speed FLC and novel estimator (red color)

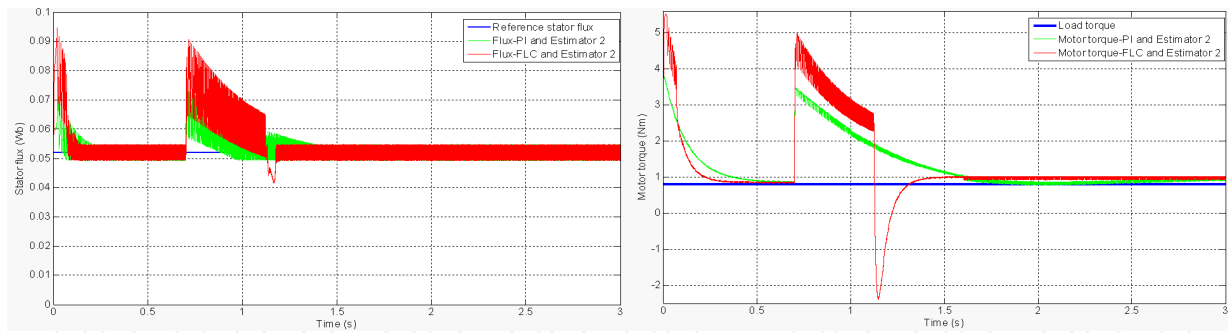


Figure 38. Motor torque (on the left) and stator flux (on the right) in case of DTC for PMSM drive using speed PI controller and novel estimator (green color), and speed FLC and novel estimator (red color)

9. Conclusion

Another solution has been presented to overcome the problems associated to DTC for PMSM in case of motor parameters variation and/or nonlinear operating conditions, which utilize speed FLC and an independent stator resistance estimator. Of course, FDTC allows rejecting the perturbations and minimizing torque and flux ripple. For all these reasons, a fixed switching frequency (DTC-SVM or DTC-SPWM) presented in this chapter can be combined with speed FLC and this independent stator resistance estimator to develop a robust DTC for PMSM.

Author details

Khalid Chikh, Mohamed Khafallah and Abdallah Saâd

Hassan II University, National Higher School of Electricity and Mechanics (ENSEM),

Department of Electrical Engineering, Energy and Electrical Systems Research Group, Morocco

10. References

- Chikh, K.; Saad, A.; Khafallah, M. & Yousfi, D. (2011a). PMSM Vector Control Performance Improvement by Using Pulse with Modulation and Anti-windup PI Controller, *Proceedings of IEEE 2011 2nd International Conference on Multimedia Computing and Systems*, pp. 1-7, ISBN 978-1-61284-730-6, Ouarzazate, MOROCCO, April 07-09, 2011
- Chikh, K.; Khafallah, M.; Saad, A. & Yousfi, D. (2011b). Drive with Low Torque and Flux Ripple for PMSM by Using Direct Torque Control with Space Vector Modulation, *Proceedings of WASET 2011 International Conference on Computer, Electrical, and System Sciences, and Engineering*, pp. 1130-1137, ISSN 2010-3778, Paris, FRANCE, June 24-26, 2011
- Chikh, K.; Khafallah, M.; Saad, A. & Yousfi, D. (2011c). A Novel Drive Implementation for PMSM by Using Direct Torque Control with Space Vector Modulation. *Canadian Journal on Electrical and Electronics Engineering*, Vol.2, No.8, (September 2011), pp. 400-408, ISSN 1923-0540

- Lokriti, AS.; Zidani, Y. & Doubabi, S. (2011). Fuzzy Logic Control Contribution to the Direct Torque and Flux Control of an Induction Machine, *Proceedings of IEEE 2011 2nd International Conference on Multimedia Computing and Systems*, pp. 1-6, ISBN 978-1-61284-730-6, Ouarzazate, MOROCCO, April 07-09, 2011
- Ningzhou, L.; Xiaojuan, W. & Xiaoyun, F. (2010). An Improved DTC algorithm for Reducing Torque Ripples of PMSM Based on Cloud Model and SVM, *Proceedings of International Conference on Multimedia Information Networking and Security*, pp. 274-277, ISBN 978-1-4244-8626-7, Nanjing, Jiangsu, November 04-06, 2010
- Pujar, HJ. & Kodad, SF. (2009). Digital Simulation of Direct Torque Fuzzy Control of PMSM Servo System. *International Journal of Recent Trends in Engineering*, Vol.2, No.2, (November 2009), pp. 89-93, ISSN 1797-9617
- Tang, L.; Zhong, L.; Fazlur Rahman, M. & Hu, Y. (2003). A Novel Direct Torque Control for Interior Permanent-Magnet Synchronous Machine Drive with Low Ripple in Torque and Flux- A Speed-Sensorless Approach. *IEEE Transactions on Industry Applications*, Vol.39, No.6, (November 2003), pp. 1748-1756, ISSN 0093-9994
- Tlemcani, A.; Bouchhida, O.; Benmansour, K.; Boudana, D. & Boucherit, M.S. (2009). Direct Torque Control Strategy (DTC) Based on Fuzzy Logic Controller for a Permanent Magnet Synchronous Machine Drive, *Journal of Electrical Engineering & Technology*, Vol.4, No.1, (December 2009), pp. 66-78, ISSN 1975-0102
- Ziane, H.; Retif, J.M. & Rekioua, T. (2008). Fixed-Switching-Frequency DTC Control for PM Synchronous Maching with Minimum Torque Ripples, *Canadian Journal on Electrical and Computer Engineering*, Vol.33, No.3/4, (December 2008), pp. 183-189, ISSN 0840-8688
- Haque, M.E. & Rahman, M.F. (2002). Influence of Stator Resistance Variation on Direct Torque Controlled Interior Permanent Magnet Synchronous Motor Drive Performance and Its Compensation, *IEEE-Industry Applications Conference-Thirty Sixth IAS annual meeting*, Vol.4, (Aout 2002), pp. 2563-2569, ISSN 0197-2618